CONF-770945--7

PREPRINT UCRL- 79834

Lawrence Livermore Laboratory

SCALING OF EXPLODING PUSHER TARGETS

JOHN H. NUCKOLLS

AUGUST 22, 1977

MASTER

THIS PAPER WAS PREPARED FOR PRESENTATION AT THE EUROPEAN CONFERENCE
ON LASER INTERACTION WITH MATTER
OXFORD, ENGLAND SEPTEMBER 19-23, 1977

SCALING OF EXPLODING PUSHER TARGETS*

John H. Nuckolls

University of California, Lawrence Livermore Laboratory
Livermore, California 94550

ABSTRACT

A theory of exploding pusher laser pusher targets is compared to results of LASNEX calculations and to Livermore experiments. A scaling relationship is described which predicts the optimum target/pulse combinations as a function of the laser power.

---

*Research performed under the auspices of the United States Energy, Research and Development Administration, Contract No. W-7405-Eng-48.

SCALING OF EXPLODING PUSHER TARGETS

J. Nuckolls

Laser fusion exploding pusher targets were invented at Livermore in 1970 for use in initial experiment.[1] We have named this type of target HYPERION. The simplest version consists of a spherical hollow glass microsphere filled with low density DT gas and mounted on a stalk. Typical microsphere parameters are 80 μm diameter, 1 μm wall thickness, and 2 mg/cm^3 DT density. Many variations of HYPERION have been developed including those in which the microsphere fusion capsule is enclosed in foam or mounted with a glass or plastic sheet.[1a] A D_2 filled glass micosphere target was first fabricated at LLL in 1970-71. The simple glass microsphere version first yielded DT neutrons in tests at KMSF in May 1974.[2] A two beam confocal ellipse illumination system was used in these experiments. Advanced HYPERIONS first generated detectable neutrons in single beam JANUS laser experiments performed at LLL in December 1974.[3] The first experimental demonstration of thermonuclear fusion in a laser implosion was achieved with advanced two beam HYPERION targets at LLL in May 1975.[4] An F/1 lens illumination system was used in these experiments. In September 1976 ARGUS two

beam experiments, advanced HYPERIONS achieved record breaking thermonuclear conditions including 8 keV ion temperatures, 10^{12} cm^{-3}s Lawson numbers, and 10^{-2} DT gains (fusion energy/DT thermal energy).[5] Figure one.

General Considerations

HYPERION targets are particularly well suited to early laser implosion experiments. Because the pusher (glass shell) is suddenly heated and exploded by a short duration ($\lesssim$ 100 ps) high power laser pulse, the implosion is relatively insensitive to preheat by superthermal electrons and x-rays and fluid instabilities grow relatively slowly. Figure 2 shows calculations of the characteristic decrease of the exploding pusher density during implosion and for comparison the behavior of a high density target. The laser temporal pulse shape may be Gaussian and the illumination may be relatively asymmetric (with some degradation in neutron yield). A variety of emissions from the imploding target make detailed diagnostics possible, including x-rays, neutrons, alpha particles, ions, and scattered light.

The HYPERION target may be imploded to thermonuclear conditions with lasers having energies as small as a few joules. With such small energies, targets weighing only a few ng can be heated to keV

temperatures at which observable fusion occurs.

The HYPERION target is designed to drive ng masses to multi-keV ion temperatures. Laser light primarily heats electrons, whereas it is the heated DT ions which generate fusion reactions. Since the ion-electron coupling time in ng masses of liquid density DT at keV temperatures is much larger than the hydrodynamic disassembly time, simple homogeneous DT pellets are poorly suited to early experiments with small lasers. For example, 10 ng of liquid density DT may be heated to 10 keV electron temperature with 4 joules absorbed energy. The ~ 100 ps is required for the electrons to heat the ions to 2 keV, whereas the hydrodynamic disassembly time is 10 ps.

The HYPERION target design overcomes this ion heating difficulty by enclosing the low density DT gas (2 mg/cm^3) in a much higher density glass microballoon. This glass and the DT gas are suddenly heated to 0.1-1 keV electron temperatures by laser heated electrons. The laser heated electron spectrum has a strong superthermal component up to 10 keV due to resonance absorption and plasma instabilities. The high thermal electron pressure in the glass causes it to explode inward and outward at high velocities (10^7-10^8 cm/s). The imploding glass ions collide with the DT ions giving the DT ions average energies ranging from several hundred electron volts to several keV.

In most experiments which have been conducted so far, the range

of these DT ions is much less than the capsule radius in the early stages of the implosion. Consequently, ion-ion collisions in the DT generate an inward moving ion shock. Behind this shock the inward moving glass continues to be heated by laser driven electrons and accelerates to higher velocities, further compressing and heating the DT ions. This post shock compression/heating of the DT ions is moderetely adiabatic, and approximately follows an adiabat with an average varying from 3/2 to 2. The fuel compression history shows moderate entropy changes due to ion-electron coupling and to energy transport by ion conduction. Figure three shows typical compression tracks in pressure-density coordinates of calculations of various exploding pusher experiments and an ablative, isentropic high gain target. In the late stages of the implosion the DT ion range may be comparable to the radius. However, the range is much shorter in the surrounding glass. The implosion culminates when the impulse generated by the compressing DT stops the inward moving glass. The DT ion temperature generally greatly exceeds the electron temperature because the rate of compressive work is much larger than the ion-electron coupling and the ion conduction is much weaker than the electron conduction.

To a first approximation the compressed DT density is proportional to that given by filling the original volume enclosed by the microballoon with the inner half of the glass mass.

Typically the DT is compressed to approximately liquid density.

Electron conduction generates a moderately symmetric implosion even if the heating is somewhat asymmetric. Multi keV laser heated electrons transport energy through the low density plasma blowing off the pellet over distances comparable to the pellet size in a time comparable to the implosion time. The classical mean free path of a 20 keV electron in Z=10 plasma at critical density for Nd light is $\sim$ 100 μm, a typical pellet diameter, and the corresponding electron velocity is $\sim 10^{10}$ cm/second. However, a significant time is required for a substantial corona region to develop and electron transport is inhibited by plasma turbulence and self-generated magnetic fields.

Plasma theory and computer simulations have successfully predicted the spectrum of superthermal electrons as a function of laser intensity and the absorption of laser light as a function of the angle of incidence and the polarization.[6] Typically, for a simple HYPERION 25% is absorbed overall, mainly via resonance absorption. For the targets with the highest neutron yields, the laser light is sufficiently intense so that inverse bremsstrahlung absorption is supressed by self-steepening of the density profile and by superthermal electron quiver velocities. More efficient absorption has been achieved with advanced HYPERION designs.

In Figure 4, the significant characteristics of exploding pusher

targets are compared to those of typical ablative isentropic high gain targets.

Scaling

A key target design objective is: for each laser power to find the optimum combination of glass dimensions, DT density, laser pulse length, and focusing. The number of parameters to be varied is sufficiently large so that it is difficult and expensive to find these optima experimentally. At LLL we have predicted the optimum designs with the LASNEX computer program (see preceding article), and concentrated most of our experiments in the region of these predicted optima. Comparison of extensive and detailed diagnostic measurements of neutron yield, DT ion temperature, implosion velocity, x-ray spectra, etc., with LASNEX calculations shows good agreement. Figures 5 and 6.

Jon Larsen has made extensive LASNEX parameter studies of exploding pusher targets.[6a] Some of these results are shown in Figures 7 and 8. For constant laser power there is a set of target/pulse parameters which give near maximum neutron yield. These optima have several striking features. The compressed DT density is nearly constant. The capsule wall thickness is nearly proportional to the radius and both increase slowly with power. The

neutron yields vary approximately with the power squared.

Absorbed Power (TW)	Neutrons
0.1	4×10^8
1	2.5×10^{10}
10	2×10^{12}

The peak DT ion temperature varies with the square of the implosion velocity and the density varies with the ratio of the wall thickness to the radius. Table I. At constant power, maximum neutron yield is achieved by a group of capsule-pulse combinations in which the DT ion temperature varies from 6 to 15 keV. Figure 9.

Published theories and semi-empirical models of exploding pusher implosions do not predict these features. In reference 7, it is assumed incorrectly that absorption is mainly by inverse bremsstrahlung (so that relatively few superthermal electrons or x-rays are generated), that the implosion is ablatively driven rather than exploding pusher, and that the imploded glass is relatively cold and dense. Consequently, the calculated DT densities increase with laser power, and are a factor of 10 to 100 fold too high. Also the ion temperatures are several fold too low. This theory does not predict the correct variation of neutron yield

TABLE I

Peak Absorbed Power (TW)	Diameter μm	Gaussian FWHM (ps)	Thickness (μm)	Peak Velocity (V_m) (μm/ps)	Peak Ion Temp (keV)	25 V_m^2 $(keV)_m$	Peak Density (g/cm³)	$16 \frac{\delta R}{R}$ (g/cm³)
.12	61	30	0.4	.66	7.9	7.9	.21	.21
.15	100	65	0.4	.36	1.4	3.2	.13	.13
.17	120	100	0.4	.36	2.8	3.2	.13	.11
.24	80	33	0.4	.62	9.7	9.6	.18	.15
.28	140	65	0.4	.40	4.0	4.0	.09	.091
.33	160	100	0.4	.42	3.9	4.4	.11	.08
.47	100	30	0.7	.58	9.6	8.4	.18	.22
.54	140	65	0.7	.46	5.6	5.3	.14	.16
.61	160	100	0.7	.42	4.3	4.4	.16	.14
1.15	140	30	0.7	.64	10.7	10.2	.16	.16
1.31	200	65	0.7	.56	8.1	7.9	.11	.11
1.47	240	100	0.7	.53	6.3	7.0	.10	.093
10.7	300	30	1	.80	11.9	16	.13	.11
11.1	350	65	1.5	.76	14.6	14.4	.13	.14
11.4	375	100	2	.76	15.0	14.4	.15	.17
11.7	450	130	1.5	.76	11.2	14.4	.10	.11
12	525	165	1.5	.70	10.1	12.3	.10	.092

with laser power or the optimum target/laser pulse combinations.

The formula in Reference 5 contains several parameters which have been adjusted to reproduce a set of LASNEX calculations. The results agree rather well with the neutron yields of most simple exploding pusher experiments which have been conducted at LLL. However, even when normalized to the LASNEX results at 0.1 and 1 TW, this formula does not correctly predict the optimum target/pulse combination at 10 TW. The predicted wall thickness is several fold too thin and the neutron yield several fold too high. The compression assumption used in this formula is seriously in error so that the predicted compressions increase with specific energy. In addition the limiting effects of electron decoupling in the shell and thermal quenching in the fuel are not included. A current version of this fomula with an improved compression assumption is described in the 1976 LLL Laser Fusion Annual Report, (in publication).

In the remainder of this article, scaling rules are developed for the set of capsules which are optimum for absorbed laser powers varying from 0.1 to 10 TW. Both hydrodynamic and transport physics

is scaled to generate these capsule-laser scaling rules.

In general, the maximum DT ion and electron temperatures, θ_i and θ_e, are related to the maximum implosion velocity, V_m, by

$$\theta_i + \theta_e \simeq 25\ V_m^2 \ ,$$

where temperatures are in keV and velocity in cm/sh (10^8 cm/s). Let p be the pressure-time impulse generated at the culmination of the implosion. Then

$$p\tau \approx \rho_g \Delta r V_m \ ,$$

where Δr is the thickness of glass which can be affected by this

impulse in time τ, ρ_g is the imploded glass density, and p is the pressure in 10^{16} ergs/cm^3. Using $\Delta r = \sqrt{\frac{p}{\rho_g}}\,\tau$, and the DT equation of state, we find

$$p \approx \rho_g V_m^2 = \frac{1}{25}\rho(\theta_i + \theta_e) \quad .$$

To a first approximation, the imploded glass immediately adjacent to the compressed DT is at the *same* pressure, temperature *and* density as the DT (due to hydrodynamics and electron and ion conduction). The decreasing pressure with radius roughly compensates for the fewer particles/mass in the glass. Consequently,

$$25\, V_m^2 \approx \theta_i + \theta_e$$

This equation is in excellent agreement with LASNEX calculations. (Table I). The electron temperature may be estimated by distributing half the absorbed energy thoughout the capsule mass. (Roughly half the absorbed energy is in hydrodynamic motion.) However, for optimum capsules which we consider here, $\theta_i >> \theta_e$ in the DT fuel.

In the implosion, the DT ions are first shocked, then compressed quasi-isentropically. Assume the matter velocity behind the initial shock is V_o and the shock compression is four fold $\left(\frac{\gamma+1}{\gamma-1} = 4 \text{ for } \gamma = 5/3\right)$. Then assume the pusher accelerates (due to isothermal blowoff) to velocity V_m, compressing the DT ions more or less isentropically to n times the original uncompressed density. If the pressure and density in the DT after passage of the first shock are p_o and $4\rho_o$, then

$$p_o = p\,\frac{2}{3}\,4\rho_o\,\frac{1}{2}\,V_o^2 \text{ , using } p = (\gamma - 1)\rho\varepsilon,\ \varepsilon = \frac{1}{2}V_o^2 \ .$$

The final pressure is $p = V_m^2$. Then using $p = p_o\left(\frac{n}{4}\right)^{\gamma}$, $\gamma = 5/3$, it follows that

$$n = 20\left(\frac{V_m}{V_o}\right)^3$$

It is implicitly assumed that the glass mass is many times larger

than the DT mass. Typcially V_o is approximately equal to the average sound speed in the glass and $V_m < 2V_o$. For $V_m^2 \simeq 2V^2$, $\eta \approx 60$ which is typical of LASNEX calculations.

When this compression equation is compared with detailed LASNEX calculations, it is found that V_G varies rapidly with radius. Also there is significant energy conduction from the shocked DT ions to the colder glass, and energy coupling to the DT electrons. Consequently γ varies from 3/2 to 2. However for the set of optimum capsules, $\gamma = 5/3$ is a good approximation.

The DT compression may also be simply approximated by filling the volume enclosed by the microballoon with the inner half of the microballoon mass. Then for an initial glass density of 2.5 g/cm^3 the average glass density is

$$\bar{\rho} \simeq \frac{\frac{1}{2}M_p}{V} = \frac{\frac{1}{2}M_p}{\rho_{o_{DT}}^{-1} M_{DT}} = 4\frac{\Delta R}{R} .$$

Because of the radial pressure gradient the central glass density is

several fold higher than $\bar{\rho}$. The DT density is proportional to the central glass density because the pressures are equalized by hydrodynamics and the temperatures by thermal conduction. Hence, the DT density, ρ, is also proportional to $\frac{M_p}{M_{DT}}$ and to $\frac{\Delta R}{R}$. Inspection of LASNEX calculations, in Table I, shows a good approximation is

$$\rho \simeq 16 \frac{\Delta R}{R}$$

The capsule and laser pulse parameters may be related by the two expressions for density derived above.

$$\rho \sim \frac{\Delta R}{R} \sim \left(\frac{V_m}{V_o}\right)^3$$

Assume the initial implosion velocity squared, V_o^2, is proportional to the energy/mass: $V_o^2 \simeq \frac{Pt_g}{R^2 \Delta R}$, where t_g is the Gaussian pulse width. Then since $V_m^2 \sim \theta_i$

$$\theta_i \sim \frac{Pt_g}{R^2 \Delta R} \left(\frac{\Delta R}{R}\right)^{2/3} \sim \frac{Pt_g}{R^3} \left(\frac{R}{\Delta R}\right)^{1/3}.$$

For the set of laser pusles and capsules which are optimally matched, we assume that t_g is proportional to the implosion time $\frac{R}{V_m}$. Since $V_m^2 \sim \theta_i$, we have

$$\theta_i^{3/2} \sim \frac{P}{R^2}\left(\frac{R}{\Delta R}\right)^{1/3}$$

Comparison with optimumn LASNEX results show good agreement.

The neutron yield, N, is given by

$$N \sim M_{DT}\rho t\,\overline{\sigma v}$$

where t is the burn time and $\overline{\sigma v}$ is the temporal and spatial average of the Maxwell velocity averaged reaction rate.

Fokker-Planck calculations have been made in the parameter space over which these capsules are being scaled. These calculations show that the DT ion distribution is sufficiently Maxwell-Boltzman so that use of $\overline{\sigma v}$ gives approximately the correct neutron yield.[8]

Depending on the imploded conditions, the burn time could be determined by hydrodynamics; thermal losses via ion-electron

coupling, radiation or conduction or by mass losses via diffusion of the hot DT into the glass. The hydrodynamic (inertial) time is

$$t_{hyd} \sim \frac{r}{C}$$

where C, the sound speed in the compressed DT fuel, varies with the square root of the ion temperature. If the inertial time were limiting, then the optimum temperature would be 15 -20 keV since the neutron yield would vary as $M_{DT}\frac{\overline{\sigma v}}{C}$ and at 15 - 20 keV $\overline{\sigma v}$ varies as the three halves power of temperature. Consequently, the optimum temperatures may be smaller than 15 - 20 keV.

As noted previously, for ng DT masses compressed to liquid densities and multi keV temperatures, neither the radiation nor the ion-electron times are limiting. This is determined by the ratios of the rate of compressive work to the rate of ion-electron coupling and to the rate of radiative cooling. The ion conduction and mass loss are limited by the rate of diffusion from the DT through the adjacent layer of hot glass into the cooler glass beyond. For the optimum capsules, θ_i is sufficiently large so that these processes cannot be neglected. Consequently, in scaling from a point on the curve at power P (in Figure 9) to one P', we require the number of ion mean free paths in the fuel to be constant. Hence

$$\frac{r}{\lambda_i} \sim \text{constant, and } \rho r \sim \theta_i^2 \text{ since } \lambda_i \rho \sim \theta_i^2$$

This is equivalent to setting the difffusion time proportional to the inertial time. The thickness of the glass "blanket" adjacent to

the imploded DT is proportional to r since the condition $V_m^2 \simeq 25\theta_i$ implies that the tamper mass approximately equals the DT fuel mass. (Conversion of the DT kinetic energy into ion thermal energy would give $V_m^2 \simeq 50\ \theta_i$ hence roughly half the DT thermal energy comes from the kinetic energy of an equal mass of adjacent glass.

Using the inertial time $\frac{r}{C}$ for the burn time t, the neutron equation is

$$N \sim M_{DT}\ \rho\ t\ \overline{\sigma v} \sim M_{DT}\ \rho r\ \frac{\overline{\sigma v}}{C}$$

Then since $\rho r \sim M_{DT}^{1/3}\ \rho^{2/3}$, and $\rho \sim \frac{\Delta R}{R}$

$$N \sim R^{10/3}\ \Delta R^{2/3}\ \frac{\overline{\sigma v}}{C}\ ,\ C \sim \theta_i^{1/2}$$

Finally we require the number of superthermal electron mean free paths in the glass shell to be constant for corresponding points on neutron vs. temperature curves with powers P and P'. However, this constant may vary slowly along each curve at constant power. This requirement is imposed because the shells are driven to the

threshold of electron decoupling, and/or energy must be transported at a sufficient rate from the critical surface to the accelerating glass-DT interface. Hence

$$\frac{\Delta R}{\lambda_e} = \text{constant}$$

where $\rho_g \lambda_e \sim \theta_{eh}^2$. The hot electron temperature θ_{eh}, is given by the flux limiter equation in LASNEX,

$$\frac{P}{R^2} \sim \theta_{eh}^{3/2}$$

Experiments and theory show θ_{eh} is proportional to the 0.4 power of the laser intensity[9] and the 0.5 power of the laser wavelength. Use of this relation instead of the flux limiter gives almost the same scaling rules if the laser wavelength is not varied. All the LASNEX calculations analyzed here were run with Nd light. In analyzing the effect of wavelength, the correct equation must be used.

When all of these conditions are used, the following scaling rules result

$$R \sim P^{4/11}$$

$$\Delta R \sim P^{4/11} \sim R$$

$$t_g \sim P^{3/11} \sim R^{3/4}$$
$$\theta_i \sim P^{2/11} \sim R^{1/2}$$

If σv varies as $\theta_i^{\,n}$ over a limited range, the

$$N \sim R^{10/3}\, \Delta R^{2/3}\, \theta_i\, n - 12$$

In the 8 - 12 keV range $n \sim 2.5$ and

$$N \sim P^{1.8}$$

With the scaling the neutron yield varies approximately with the square of the laser power in agreement with LASNEX calculations. In Table II these scaling rules are used to generate results at 12 TW and .12 TW starting from a LASNEX calculation at 1.2 TW (point 3 in

Figure 9). For comparison similiar LASNEX calculations at 12 and .12 TW are also shown (points 6 and 0).

TABLE II

#	R(μm)	R(μm)	t_g(ps)	θ_i(keV)	N
3(1.2 TW LASNEX)	80	1	65	12	2.4×10^{10}
-(12.5 TW SCALE)	184	2.3	122	18	1.5×10^{12}
6(11.4 TW LASNEX)	188	2	100	15	1.9×10^{12}
-(0.125 TW Scale)	35	0.43	35	8	3.7×10^{8}
(0.12 TW LASNEX)	30	0.4	30	7.9	3.2×10^{8}

The lower temperature LASNEX calculation in Figure 5 are also rather well related by the scaling rules as shown in Table III.

TABLE III

#	R(μm)	ΔR(μm)	t_g(ps)	θ_i(keV)	N
1(1.47 TW LASNEX)	120	0.7	100	6.3	2.3×10^{10}
-(12.5 TW SCALE)	262	1.5	180	6.3	2.3×10^{10}
4(12 TW LASNEX)	262	1.5	165	10.0	2.0×10^{12}
2(1.3 TW LASNEX)	100	0.7	65	9.1	2.2×10^{12}
-(12.5 TW SCALE)	230	1.5	122	12.3	1.4×10^{12}
6(11.7 TW LASNEX)	225	1.5	130	13.2	2.0×10^{12}

The relatively weak dependence of neutron yield on peak ion temperature in the 6-15 keV range for powers ≥ 1 TW may be understood as follows. The neutron yield is given by

$$N \sim R^{10/3}\ \Delta R^{2/3}\ \theta_i^{\,2},\quad 7 < \theta_i < 14\ \text{keV}$$

and Θ_i is given by

$$\theta_i \sim \frac{P t_E}{R^3}\left(\frac{R}{\Delta R}\right)^{1/3} \sim \frac{P}{R^2 \theta_i^{1/2}}\left(\frac{R}{\Delta R}\right)^{1/3} \quad \text{using } R \sim \theta^{1/2} t_E$$

Therefore, for constant P

$$\theta_i^{\,3} \sim R^{-10/3}\ \Delta R^{-2/3}$$

and

$$N \sim \theta_i^{-3}\,\theta_i^{2} \sim \theta_i^{-1}, \quad 7 < \theta_i < 14 \text{ keV}$$

Hence the variation in neutron in this temperature range should be only two fold and the optimum ion temperature is somewhat less than 10 keV.

Inspection of the LASNEX calculations shows that the number of electron mean free paths in the pusher, the number of ion mean free paths in the compressed fuel, and temperature decreases at constant power (Table 4). The ratios are normalized to those of #3.

TABLE IV

#	θ_i	$\frac{R}{\Delta R}$	$\frac{r}{\lambda_i}$	$\frac{\Delta R}{\lambda_e}$	$\frac{\theta_i R^3}{Pt_E}\left(\frac{\Delta R}{R}\right)^{1/3}$
1	6.3	2.1	3.3	2	0.9
2	8.1	1.7	1.8	1.25	1.05
3	12	1	1	1	1
4	10.1	2.1	2.7	2	.86
5	13.2	1.9	1.5	1.15	.96
6	15	1.2	1.3	1	.98

At the highest temperatures, some thermal quenching of the burn is occurring, so that the neutron yield is slightly increased by moderately increasing $\frac{r}{\lambda_i}$ as θ_i is reduced. However $\frac{r}{\lambda_i}$ and $\frac{\Delta R}{\lambda_{eh}}$ are coupled and must increase together. Using

$$\rho\lambda_i \sim \theta_i^2,\ \rho_g\lambda_{eh} \sim \theta_{eh}^2,\ \frac{P}{R^2} \sim \theta_{eh}^{3/2},\ \frac{P}{R^2}\left(\frac{R}{\Delta R}\right)^{1/3} \sim \theta_i^{3/2},$$

it follows that

$$\frac{\frac{\Delta R}{\lambda_{eh}}}{\frac{r}{\lambda_i}} \sim \left(\frac{R}{\Delta R}\right)^{1/9}$$

which is nearly constant since $\frac{R}{\Delta R}$ varies two fold. However, increasing $\frac{\Delta R}{\lambda_{eh}}$ reduces electron energy transport to the glass-DT interface, and results in less efficient use of the laser energy. The combined effect of changing θ_i, $\frac{r}{\lambda_i}$, and $\frac{\Delta R}{\lambda_{eh}}$ in a self consistent way results in nearly constant neutron yield for $7 < \theta_i < 15$ keV with $P \geq 1$ TW. Figure 10 shows Figure 9 with contours of equal numbers of mean free paths superimposed. The optimum LASNEX results form a simple and beautiful pattern determined by basic physical processes.

Possible sets of scaling rules at constant power are still being analyzed. Tentatively, a fairly good set is

$$\theta_i \sim \left(\frac{\Delta R}{R}\right)^{2/3} P^{2/11}$$

$$\frac{r}{\lambda_i} \sim \frac{P^{4/11}}{\theta_i^2} \sim \frac{\rho r}{\theta_i^2}; \quad \rho r \sim P^{4/11}$$

$$\frac{R}{\lambda_{eh}} \sim \frac{r}{\lambda_i}\left(\frac{R}{\Delta R}\right)^{1/9}$$

The existence of an optimum initial DT density, ρ_o, follows from two competing effects. Increasing ρ_o increases M_{DT}, but decreases the DT ion temperature. Since the neutron yield is proportional to both the DT mass and to some power of the ion temperature (via $\overline{\sigma v}$), there is an optimum initial DT density. The near invariance of this optimum density for the capsules considered here follows from several considerations: the weak dependence of ion temperature on density; DT thermal quenching and mass loss limits on the ion temperature; and the ion temperatures being below the 15 - 20 keV optimum. For the 10 TW absorbed calculations where the ion temperature approaches 15 -20 keV, LASNEX shows the optimum initial density has begun to increase and is 5×10^{-3} g/cm^3. From these considerations a steady increase in the optimum ρ_o is expected for higher laser powers.

For suboptimal exploding pusher capsule-pulse combinations, these scaling fuels may not apply. The pulse capsule mismatch may be compensated for by use of the effective absorbed energy approximation is reference 5. However, this approximation has limited validity. Implosions in which the pusher does not explode also follow different scaling rules.

Figure Captions

Figure One — DT ion temperatures, Lawson numbers, and DT gains achieved in LLL laser fusion experiments with HYPERION targets. The Lawson number is the product of the electron density and confinement time, and the DT gain is the ratio of the fusion energy generated to the thermal energy in the DT ion and electrons. Performance of various magnetic fusion machines is also shown.

Figure Two — Maximum density in HYPERION glass microballoons vs. radius/initial radius. Explosion of glass to lower densisty drives the implosion of the DT fuel. Also shown for comparison is projected performance of typical high density target.

Figure Three — Pressure density tracks followed by DT fuel in LLL laser fusion experiments with HYPERION targets. Maximum ion temperatures are also indicated. Curvature is due to energy coupling to DT electrons and to ion conduction to glass. Projected tracks for typical high density target are also shown.

Figure Four — Comparison of HYPERION exploding pusher low density, target parameters and those projected for typical high density targets.

Figure Five — Comparison of LASNEX predictions of neutron yield with experimental measurements for a series of HYPERION targets imploded by the *JANUS* and *ARGUS* Nd glass lasers.

Figure Six — Comparison of LASNEX predictions of various parameters of exploding pusher target implosions with experimental measurements.

Figures Seven and Eight — Results of LASNEX parameter studies of exploding pusher targets imploded with spherically symmetries laser pulse.

Figure Nine — Optimum capsule - pulse combinations at absorbed laser powers of 0.12, 1.2, and 12 TW vs. DT ion temperature. Table shows capsule radius and wall thickness and laser pulse width (Gaussian FWHM).

Figure Ten — Figure 5 with contours of equal numbers of mean free paths and scaling results. Note that #3 and #6 are not scaling pairs. The key role of transport processes in scaling is obvious.

Figure Eleven — Domain in R, ΔR space of the set of exploding pusher capsules having maximum neutron yield at constant laser power. Processes bounding this domain are indicated.

THERMONUCLEAR CONDITIONS ACHIEVED IN FUSION EXPERIMENTS

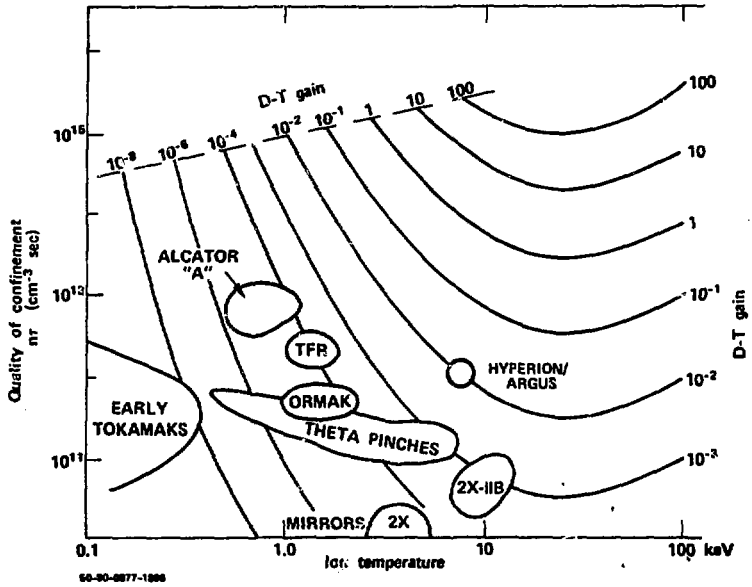

PUSHER DENSITY HISTORIES OF VARIOUS TARGETS

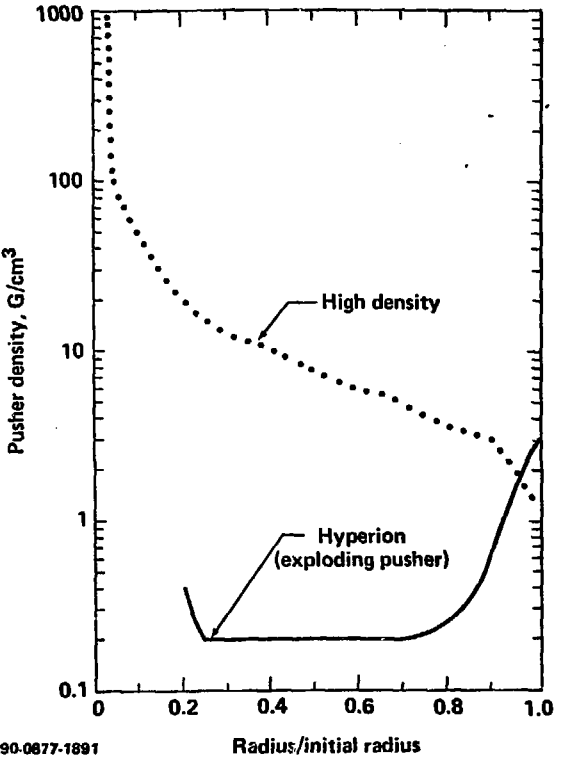

50-90-0677-1891

PRESSURE-DENSITY TRACKS OF LASER FUSION TARGET DESIGNS

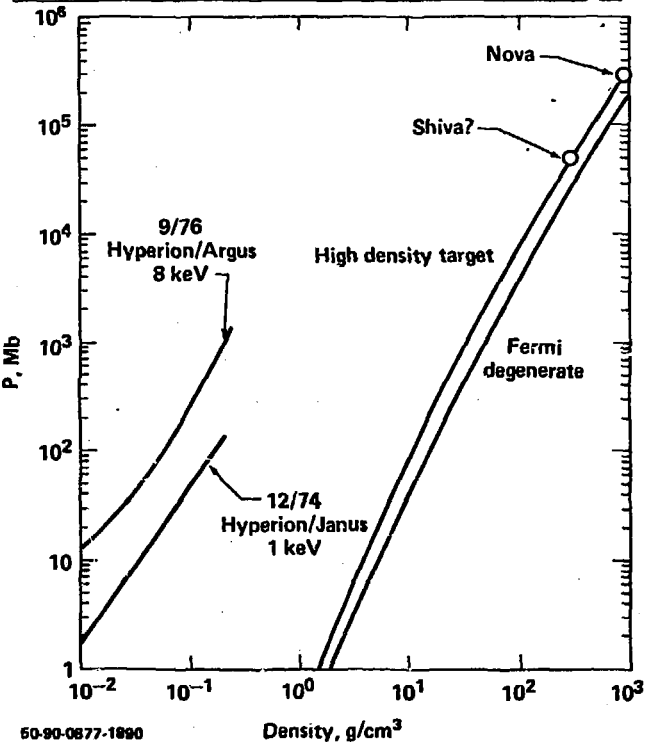

50-90-0877-1890

Figure 4

	EXPLODING PUSHER	HIGH DENSITY
Fuel Compression (x liquid)	0.1 - 10	300 - 10,000
Fuel Temperature (keV)	1-20 keV	10 - 100 keV
Implosion Velocity (cm/s)	$1-10 \times 10^7$	$2 - 6 \times 10^7$
Gain	$10^{-6} - 10^{-1}$	$10^{-2} - 100$
Fuel State (initial)	Low density gas	Cryogenic shell
Surface Finish	1000 A	100 - 1000 A
Fluid Instabilities	insensitive	sensitive
Pulse Shape	Gaussian	5 Step
Entropy Change	High	near isentropic
Laser Energy/Power	10 J/0.1 TW	10 KJ/30 TW
Symmetry Sensitivity	least	high
Preheat Sensitivity	least	high

NEUTRON YIELDS – EXPERIMENTS VS LASNEX

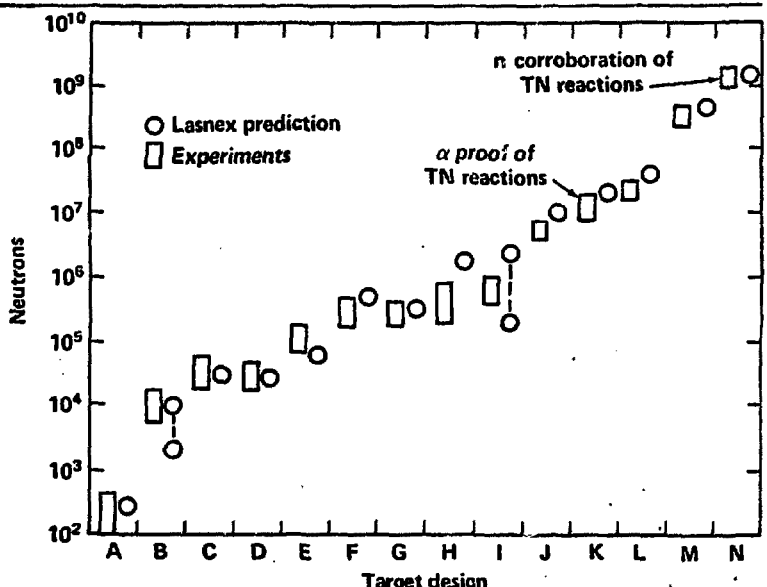

LASER IMPLOSIONS – COMPARISON OF EXPERIMENTS AND CALCULATIONS (LASNEX)

Quantity	Experiment	LASNEX	Laser	Focusing	Target	Diagnostic
Neutron yield	$1\text{-}2 \times 10^9$	2×10^9	ARGUS	2 F/1 lenses	Complex	Cu activation, scintillator PMT
Alpha energy (MeV)	3.3	3.3	JANUS/ ARGUS	2 F/1 lenses	Complex	αTOF
Ion temperature (keV)	6 - 10	8	ARGUS	2 F/ lenses	Complex	η, α TOF
Implosion velocity (cm/s)	3×10^7	3.3×10^7	JANUS	Confocal	Ball	Streaked X pinhole, X streaking
Density (g/cm^3)	0.1 - 0.2	0.1 - 0.2	JANUS/ ARGUS	2 F/1 lenses	Ball/ complex	X-ray microscope
Absorbed energy (%)	20 - 25	20 - 25	JANUS/ ARGUS	F/1 and confocal	Ball	Calorimeter, ions, diode array

EXPLODING PUSHER NEUTRON YIELD AS A FUNCTION OF TARGET PULSE WIDTH AND LASER POWER

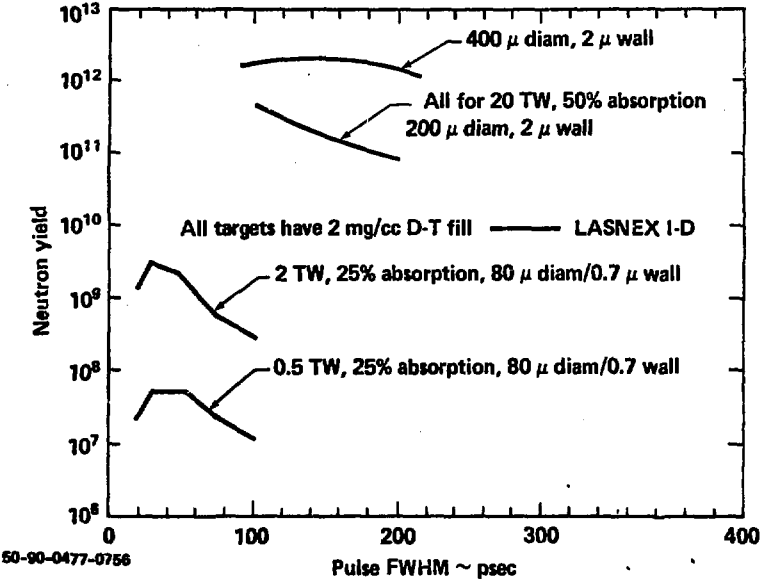

50-90-0477-0756

OPTIMUM HYPERION TARGETS WITH 1.0 MICRON WALL

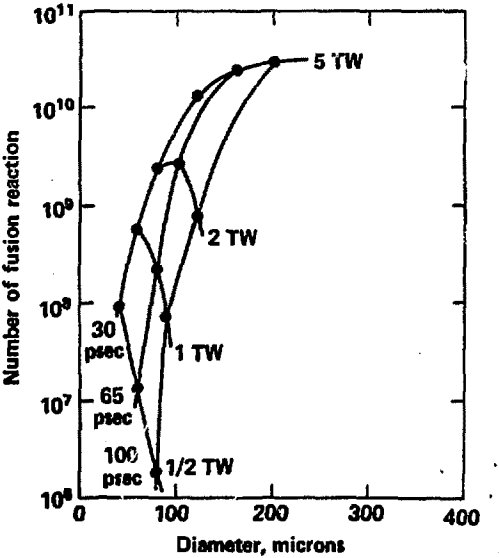

OPTIMUM NEUTRON YIELDS VERSUS DT ION TEMPERATURE

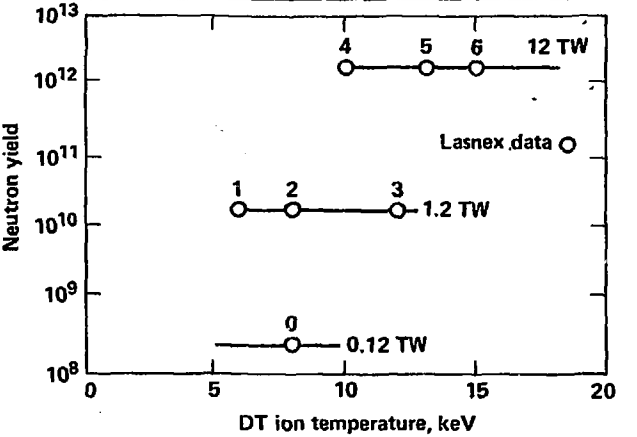

	Power	Radius	Thickness	Pulse width	N
6	11.4	188 μm	2 μm	100 ps	1.9×10^{12}
5	11.7	225	1.5	130	2×10^{12}
4	12	262	1.5	165	2×10^{12}
3	1.2	80	1	65	2.4×10^{10}
2	1.31	100	0.7	65.	2.2×10^{10}
1	1.47	120	0.7	100	2.3×10^{10}
0	0.12	30	0.4	30	3.7×10^{8}

50-90-0877-1888

OPTIMUM NEUTRON YIELDS VERSES DT ION TEMPERATURE

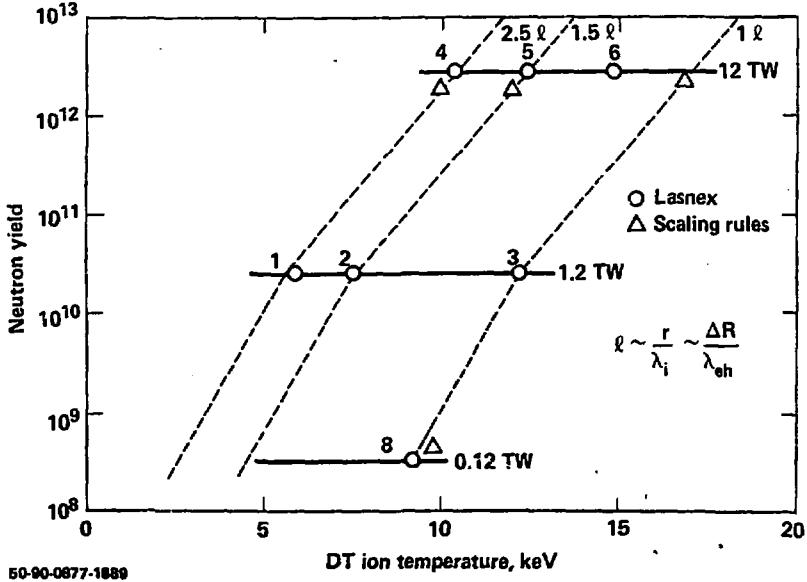

50-90-0677-1889

R, ΔR DOMAIN OF SET OF EXPLODING PUSHER CAPSULES HAVING MAXIMUM NEUTRON YIELD AT CONSTANT LASER POWER

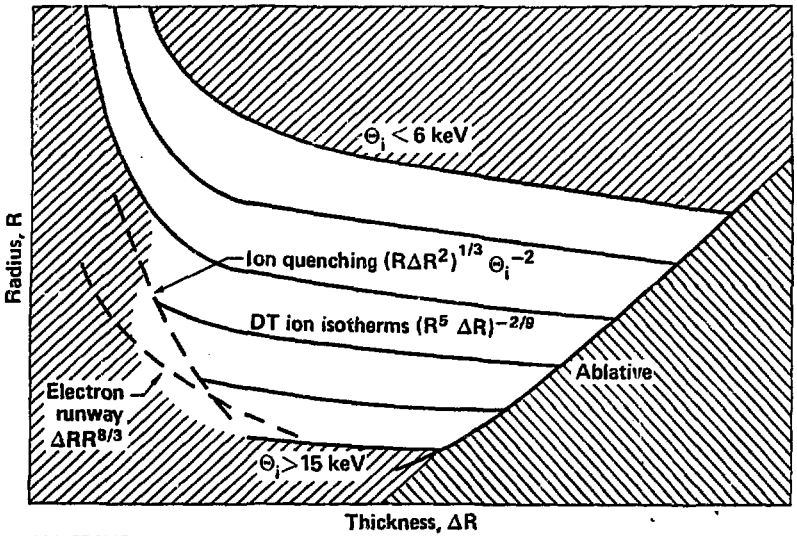

50-90-0877-1887

REFERENCES

1. J. H. Nuckolls, UCRL-50,000 71-5, 1971, SRD. This material was presented to the President's Scientific Advisory Committee on Dec. 15, 1970, and to the AEC General Advisory Committee, Dec. 16, 1970.

1a. G. H. McCall, R. Morse, Laser Focus Magazine, Dec. 1974.

2. G. Charactis, et.al., Plamsa Physics and Controlled Nuclear Fusion Research IAEA, Vol. II, p. 317, 1975.

3. J. H. Nuckolls, UCRL-76395, 1975. Also published in "Progress in Laser Fusion," Plenum Press, N.Y., 1975, p. 105.

4. V. W. Slivinsky, et.al., Phys. Rev. Lett., 35, 1083 (1975).

5. E. K. Storm, et.al., UCRL-79031, 1976. Submitted to Phys. Rev. Lett.

6. K. G. Estabrook, et.al., Physics of Fluids, Vol. 18, #9, 1975, p.1151.

6a. J. Larsen, 1976 Laser Fusion Annual Report, Lawrence Livermore Laboratory, (in publication).

7. K. A. Brueckner, Nucl. Fusion, 16, 3 (1976) p. 387.

8. G. B. Zimmerman, UCRL-76927, (1975).

9. D. V. Giovanelli, Bull. Am. Phys. Soc., (1976), p. 1047.